Journal of Sound and Vibration 431 (2018) 276–294

Contents lists available at ScienceDirect

Journal of Sound and Vibration

journal homepage: www.elsevier.com/locate/jsvi

A model for simulating vibration responses of grinding machine-workpiece-hand-arm systems

Ren G. Dong [a, *], Daniel E. Welcome [a], Xueyan Xu [a], Qingsong Chen [b], Hansheng Lin [b], Thomas W. McDowell [a], John Z. Wu [a]

[a] Engineering & Control Technology Branch, Health Effects Laboratory Division, National Institute for Occupational Safety and Health, Morgantown, WV 26505, USA

[b] Guangdong Province Hospital for Occupational Disease Prevention and Treatment, Guangdong Provincial Key Laboratory of Occupational Disease Prevention and Treatment, Guangzhou, Guangdong, China

ARTICLE INFO

Article history:
Received 22 December 2017
Received in revised form 1 June 2018
Accepted 4 June 2018

Handling Editor: J. Macdonald

Keywords:
Hand-arm vibration
Hand-transmitted vibration
Handheld workpiece vibration
Vibration-induced white finger
Hand-arm vibration model

ABSTRACT

The objective of this study was to develop a vibration model of a grinding machine-workpiece-hand-arm system. A lumped-parameter model structure of the system was proposed, and its major parameters were determined using the mechanical impedance measured at the grinding point of a typical workpiece (golf club head) held by two hands and referenced to the vibration transmissibility spectra measured at the wrist and on the upper arm of human subjects. The model reasonably predicted the vibration transmissibility spectra measured on the club head and the driving-point response function when the grinding contact stiffness was below a certain value. This suggests that the model is acceptable not only to enhance the understanding of the system responses, but also to explore some engineering methods for controlling vibration exposures during the grinding process. The identified model parameters reveal that the major resonance of the handheld workpiece depends primarily on its mass and grinding contact stiffness. The feed force applied in the grinding process can substantially affect the grinding contact stiffness; as a result, it can significantly influence the resonance. Vibration-reducing gloves can marginally increase the workpiece resonance, but these gloves can reduce some vibration transmitted to the hand-arm system. This study also clarified an important mechanism for the prediction errors of linear human vibration models, which is useful to further improve human vibration modeling.

Published by Elsevier Ltd.

1. Introduction

Grinding and polishing of handheld workpieces are manual processes used in the fabrication or repair of some components of sports equipment, tools, furniture, and dentures [1–3]. Significant vibration may be generated during such processes, and the vibration may be effectively transmitted to the fingers or hands of the workers holding the workpieces. Such vibration exposure may cause vibration-induced white finger (VWF), a form of Raynaud's Syndrome, and a significant cause of morbidity [4]. A recent study found a significant prevalence (>12%) of VWF among workers performing the fine grinding of

* Corresponding author. ECTB/HELD/NIOSH/CDC, 1095 Willowdale Road, MS L-2027, Morgantown, WV 26505, USA.
E-mail address: rkd6@cdc.gov (R.G. Dong).

https://doi.org/10.1016/j.jsv.2018.06.008
0022-460X/Published by Elsevier Ltd.

golf club heads in some sports equipment factories [3]. Effective methods are required to reduce the vibration exposure to control this occupational disease among workers.

As part of the efforts towards controlling the vibration exposure of workers performing the grinding and polishing of golf club heads, an experimental study has been conducted to identify the basic vibration characteristics of the handheld workpieces made at a sports equipment manufacturer [5]. The study confirmed that the vibration of a handheld workpiece generally resulted from two types of vibration sources: (i) the vibration generated on the machine and transmitted to the workpiece; and (ii) the grinding vibration generated at the grinding interface. The machine vibration is highly correlated with the frequency-weighted vibration of the club head [5], which is required for assessing the risk of the vibration exposure in the standard method [4]. The grinding force generated at the grinding interface can result in substantial high-frequency vibration, which can also be effectively transmitted to the hands holding the club head during the grinding process. Many studies suggested that such high-frequency vibration should not be ignored for assessing the risk of VWF [6–11]. Therefore, both frequency-weighted and unweighted vibrations should be controlled in the grinding operations. While several engineering methods have been proposed to control the exposure, they have not been sufficiently evaluated. A systematic analysis of these methods requires a valid model of the grinding machine-workpiece-hand-arm system, but the literature search towards this study did not find such a model.

In principle, the required model can be constructed by combining a grinding machine model, a workpiece model, and a hand-arm-system model [12], similar to those used to simulate the vibration response of a tool-handle-hand-arm system [13–16]. While it is extremely difficult to analyze all the potential methods using a single model, the current study will focus on the development of the model for analyzing the engineering controlling methods associated with the vibration responses of the workpiece-hand-arm system. This avoids the need to simulate the detailed machine structure and grinding mechanisms. Then, the machine can be crudely simulated as a lumped-parametric structure, and the machine vibration can be generalized as a random-excitation input to the interface between the machine and workpiece.

The detailed biodynamic responses, such as the vibration stresses and strains of the hand-arm system, are not essential information for the analysis of the vibration control methods, but the overall vibration of the workpiece and that transmitted to the hand-arm system are critical for the evaluation of these methods. For this reason, it is not necessary to simulate the detailed responses of the hand-arm system, but its impedance or mechanical-equivalent model can be used to simulate the effect of the system on the workpiece response, similar to that used to analyze the tool responses [12,15,16]. Many such models are available [12–19], but they cannot be directly used in the current study, because their parameters were determined based on the biodynamic response functions of the hand-arm system with some specific arm postures and hand-handle coupling conditions that are largely different from those used in the grinding of handheld workpieces. The required model parameters should be determined based on the response functions of the dual hands-arms system with representative arm postures and hand-workpiece coupling conditions used in the grinding process [19,20]. The experiment required for the measurement has been conducted in our previous study [21].

Based on this background, the specific aims of the current study are to develop a model of the grinding machine-workpiece-hand-arm system using the available experimental data and to enhance the understanding of the vibration responses of the system. Some additional experiments are also conducted in the current study to evaluate the validity and usefulness of the model proposed and calibrated in this study. Based on the knowledge developed in this study, a few strategic approaches for reducing the vibration exposure in the grinding of handheld workpieces are also proposed and discussed.

2. Method

An inverse dynamic method based on frequency response functions was used to develop the model of the grinding machine-workpiece-hand-arm system. A previous study proposed a set of validation criteria for the development of human vibration models using this approach [20]. Those criteria were used as a general guide for the model development performed in this study.

2.1. General considerations and basic model structure

Belt grinding machines are widely used in the fine grinding of many handheld workpieces, and they are considered in this study. Fig. 1(a) shows such a machine used to grind a typical handheld workpiece – a golf club head. A schematic of its basic mechanism of operation is shown in Fig. 1(b). The grinding process is usually conducted on the drive wheel on the machine. The drive wheel is equipped with a rubber tread with inclined strips or teeth, which provides sufficient frictional force to drive the grinding belt subjected to tangential grinding force. The rubber tread is replaced with a new one when its strips are worn out by the grinding belt. The rubber tread also provides a certain cushion to avoid impacts during the grinding contact so that the fine grinding can be stable and smooth to achieve the desired quality of the product.

In the previous experimental study [5], the vibrations in three orthogonal directions (3-D) on two grinding machines and two handheld workpieces were measured. It was found that the vibration spectra in the three directions on each machine were highly correlated ($r > 0.90$, $p < 0.001$). The three axial vibration spectra measured on each workpiece were also highly correlated. These similarities suggest that the vibrations in the three directions resulted from the same excitations, and the basic mechanisms of the vibration transmission and system responses in all the directions were similar. Therefore, it is not necessary to simulate the coupled 3-D vibration responses of the system if the purposes of the modeling are to help

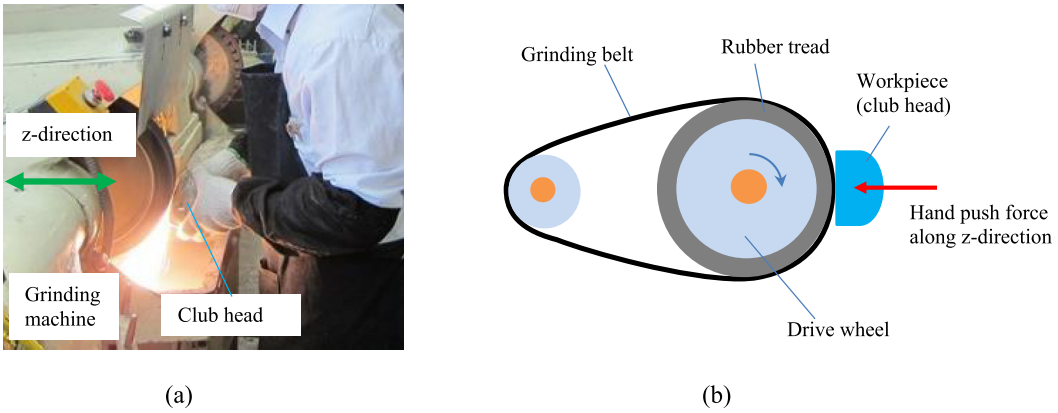

Fig. 1. The grinding of a handheld workpiece (golf club head) on a belt grinding machine with an elastic tread on its drive wheel: (a) a worker in a fine grinding operation; (b) the mechanism of the belt grinding machine.

understand the basic vibration characteristics of the system and to apply the model to explore and qualitatively analyze the vibration-reducing methods. For this reason, only the vibration responses of the system along the z-direction (horizontal axis through the center of the drive wheel and perpendicular to the plane formed by the vertical axis and wheel shaft axis) shown in Fig. 1 were simulated in this study. It was felt that determination of the additional dimensions was unnecessarily duplicative, and would needlessly complicate the designs of the experiment and model.

The proposed basic model of the machine-workpiece-hand-arm system is shown in Fig. 2. It has five Degrees of Freedom (DOFs) (z_w, z_c, z_f, z_a, and z_u). Because the machine body vibration was not substantially affected by the grinding process [5], it is not necessary to consider the entire machine to simulate the vibration transmissions in the drive-wheel-workpiece-hands-arms system; only the drive wheel is essential. It was simulated using a mass (m_w) with a generalized coordinate of z_w. Its connections to the machine body and ground were simulated using a spring (k_2) and a damper (c_2). While the mass of the rubber tread was partially lumped to the drive wheel and partially to the club head, its elastic and damping properties were represented using another spring (k_1) and damper (c_1) pair that connected the drive wheel to the club head. No obvious natural resonance of the club head itself was found in the measured response spectra [21]. Therefore, the club head was simulated as a lumped mass (m_c) with a generalized coordinate of z_c in the model, as shown in Fig. 2.

Although the machine vibration may result from various sources, it is transmitted to the workpiece through or from the drive wheel. Therefore, it was generally represented using an excitation force (F_W) acting on the drive wheel. The excitations input to the system at the grinding interface include those from the geometrical irregularities on the drive wheel tread and the complex unstable cutting of the grinding process, which may also be influenced by the machine vibration and system responses. Because it is very difficult to directly simulate these excitation sources in the linear model considered in this study, their effects were represented by the vibration force acting at the interface. Similar to lumping the mass of the interface materials to the two interacting bodies simulated in the model, the interface vibration force was lumped partially to the excitation force on the drive wheel (F_W) and partially to that acting on the club head (F_C), which is also shown in Fig. 2.

As shown in Fig. 1(a), both hands are effectively involved in the grinding process of the golf club head. For the purpose of this study, it is difficult and unnecessary to consider them separately in the simulation. They were simulated using a mechanical-equivalent model that can simulate the impedances distributed at the fingers and palm of the hand [17]. It has three DOFs or three mass elements: m_f for the fingers, m_a for the palm-wrist-forearm substructures, and m_u for the upper arm. The major components of the club head vibration are usually at frequencies of 20 Hz or above [5]. Because they are much higher than the fundamental resonant frequency (2–10 Hz) of the entire human body, and the vibration components at frequencies above 20 Hz cannot be effectively transmitted to the substructures beyond the upper arm [22], the remaining substructures of the human body were considered a mass fixed on the ground plane.

The hand-arm system is generally a time-dependent nonlinear system. Similarly, the stiffness and damping properties of the rubber are also generally nonlinear, which are affected by the grinding contact geometries and feed force. While it is extremely difficult to accurately simulate the workpiece-hand-arm system, this study hypothesized that the system could be approximately considered as a linear system within a certain vibration range, including the grinding contact interface. This hypothesis was tested in this study. With the linear hypothesis, the equations of motion of the system model are expressed as follows:

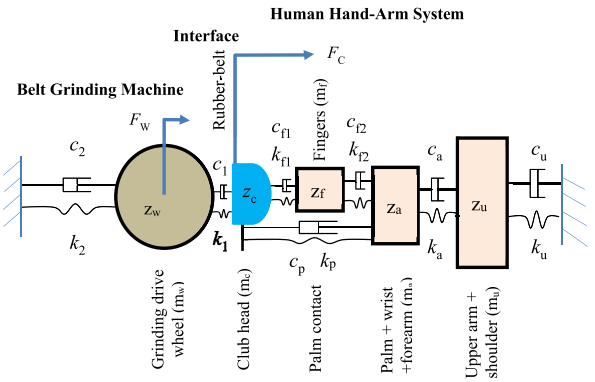

Fig. 2. The proposed model of a grinding-machine-workpiece-hand-arm system.

$$\begin{bmatrix} m_w & 0 & 0 & 0 & 0 \\ 0 & m_c & 0 & 0 & 0 \\ 0 & 0 & m_f & 0 & 0 \\ 0 & 0 & 0 & m_a & 0 \\ 0 & 0 & 0 & 0 & m_u \end{bmatrix} \begin{Bmatrix} \ddot{z}_w \\ \ddot{z}_c \\ \ddot{z}_f \\ \ddot{z}_a \\ \ddot{z}_u \end{Bmatrix} + \begin{bmatrix} c_1+c_2 & -c_1 & 0 & 0 & 0 \\ -c_1 & c_1+c_{f1}+c_p & -c_{f1} & -c_p & 0 \\ 0 & -c_{f1} & c_{f1}+c_{f2} & -c_{f2} & 0 \\ 0 & -c_p & -c_{f2} & c_{f2}+c_a+c_p & -c_a \\ 0 & 0 & 0 & -c_a & c_a+c_u \end{bmatrix} \begin{Bmatrix} \dot{z}_w \\ \dot{z}_c \\ \dot{z}_f \\ \dot{z}_a \\ \dot{z}_u \end{Bmatrix}$$
$$\begin{bmatrix} k_1+k_2 & -k_1 & 0 & 0 & 0 \\ -k_1 & k_1+k_{f1}+k_p & -k_{f1} & -k_p & 0 \\ 0 & -k_{f1} & k_{f1}+k_{f2} & -k_{f2} & 0 \\ 0 & -k_p & -k_{f2} & k_{f2}+k_a+k_p & -k_a \\ 0 & 0 & 0 & -k_a & k_a+k_u \end{bmatrix} \begin{Bmatrix} z_w \\ z_c \\ z_f \\ z_a \\ z_u \end{Bmatrix} = \begin{Bmatrix} F_W \\ F_C \\ 0 \\ 0 \\ 0 \end{Bmatrix} \quad (1)$$

2.2. Determination of the model parameters

While the drive wheel mass and the club head mass can be directly measured, it is difficult to directly measure the other parameters of the system model shown in Fig. 2. This study used a model calibration method to determine the remaining parameters, except k_2 and c_2, using measured frequency response functions (mechanical impedance and vibration transmissibility) of the system subjected to the excitation resulting from F_W, similar to those widely used in the human vibration modeling [12–14,17–20]. While k_2 and c_2 cannot be determined in the model calibration using these reference functions, and their actual values do not affect the calibration of the other parameters, a parametric study was conducted to estimate their effects on the vibration responses of the system when F_C was applied to predict the system responses.

2.2.1. Experimental data used for the calibration of the model

The reference functions required for the model calibration were measured in a recently reported study [21]. Briefly, ten healthy adult subjects (5 males with mean weight of 80.8 kg and mean height of 175.5 cm; 5 females with mean weight of 67.7 kg and mean height of 163.5 cm) participated with informed consent in the experimental study, the majority of whom were college students. The study protocol was reviewed and approved by the NIOSH Human Subjects Review Board. The basic test setup is shown in Fig. 3(a). A random excitation from 6.3 to 1600 Hz was used as the excitation in the experiment, which was an extension of the vibration spectrum defined in ISO 10819 for the standard anti-vibration glove test [23]. Unlike the instrumented handles used for the measurement of the biodynamic responses of the hand-arm system, the handle used in the measurement had a measuring cap with a flat surface, which provided a secure attachment of a rubber pad on the surface for simulating the rubber tread of the drive wheel and a stable contact of the club head on the handle (Fig. 3(b)). Three different rubber pads were used to represent three levels of grinding contact stiffness (Low = thicker pad + rubber bands; Medium = thinner pad + rubber bands; High = rubber bands only) in the experiment to examine the basic effects of the overall contact stiffness on the vibration characteristics of the club head-hand-arm system. Two levels of feed force (15 N and 30 N) were also used in the experiment to examine the feed force effects. Two hand conditions (bare hands and gloved hands) were considered to examine the glove effects. Similar to that shown in Fig. 1(a), each subject used two hands to hold a typical stainless steel golf club head and applied a given feed force on the club head against the handle interface in the horizontal direction, as shown in Fig. 3(a). The apparent mass of the system along the z-direction was evaluated using the dynamic force and acceleration measured on the instrumented handle. After subtracting the tare mass of the instrumented handle, the apparent mass was used to calculate the mechanical impedance of the interface-workpiece-hand-arm system. As also shown in Fig. 3(a), the vibrations transmitted to the club head, hand dorsum, wrist, forearm, and upper arm were also measured using instrumented adapters [21], which were used to calculate the vibration transmissibility spectra. All of the measured frequency response functions were expressed in the one-third octave bands in the frequency range of 6.3 to 1600 Hz [21].

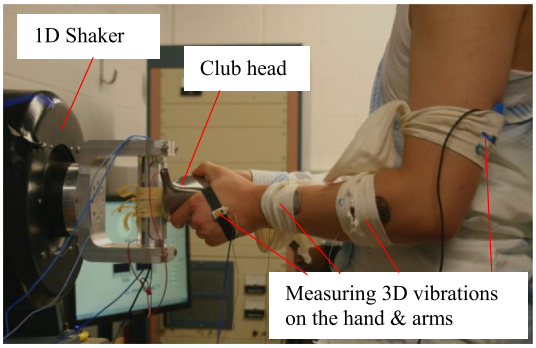

(a)

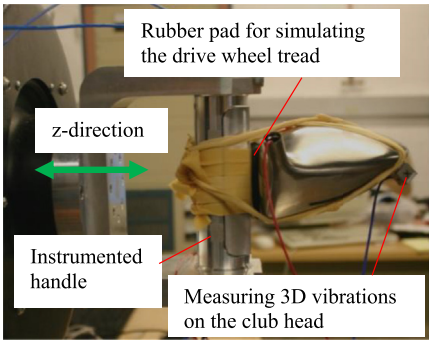

(b)

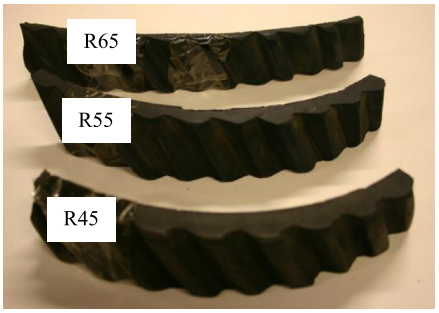

(c)

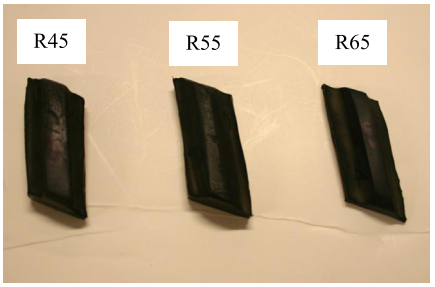

(d)

Fig. 3. The measurement of the response functions of the interface-workpiece-hand-arm system subjected to vibration along the horizontal direction on a single-axis vibration test system equipped with an instrumented handle [21]: (a) test setup and subject posture; (b) club head test; (c) samples of real rubber treads cut from drive wheels at a workplace; (d) rubber pads cut from the sample treads.

As also shown in Fig. 3(a), the hands and arms are not aligned with the z-direction or the vibration direction of the shaker. It is also very difficult to align the accelerometers attached on the club head and hand-arm system with the shaker vibration direction. For these reasons, a tri-axial accelerometer was used to measure the 3-D vibrations at every measuring location on the system, including that on the instrumented handle [21]. The vibration transmissibility (T_L) relative to the handle at each frequency for each location on the system was calculated from the measured 3-D vibration accelerations (a_x, a_y, a_z) in the local coordinate system using the following formula:

$$T_L = \frac{\sqrt{a_{x-L}^2 + a_{y-L}^2 + a_{z-L}^2}}{\sqrt{a_{x-Handle}^2 + a_{y-Handle}^2 + a_{z-Handle}^2}} \qquad \text{L: club head, wrist, and upper arm} \tag{2}$$

The validity of the total vibration method was examined by comparing the club head transmissibility measured using the tri-axial accelerometer method and that measured using laser vibrometers (PSV-300 and PDV-100, Polytec, Berlin, Germany) aligned with each measurement axis [21]. As shown in Fig. 3(b), the club head was secured on the instrumented handle using 30 N force provided by two sets of generic rubber bands (with effective mass < 2 g) in the measurement [21]. The three levels of contact stiffness simulated with the rubber interfaces were also used in the experiment. The apparent mass and transmissibility spectra of the club head in all the directions were simultaneously measured. The total vibration transmissibility spectrum agreed very well with that measured with the laser vibrometer in the z-direction with little cross-axial vibration observed in the other axes. This was not the case when the club head was not tightly and stably fixed on the handle. In such a case, the total vibration transmissibility was marginally greater than that measured with the laser vibrometer. This, however, did not affect the basic characteristics of the vibration transmissibility [21].

2.2.2. Procedures for calibrating the unknown model parameters

The above-described experiments simulated the vibration responses of the workpiece-hand-arm system subjected to the excitation from the drive wheel (F_w). The measured response functions were used to calibrate the model. The specific

references used in the calibration included the following three sets of functions: (i) the real and imaginary parts of the mechanical impedance ($Z_{z\text{-Re}}$ and $Z_{z\text{-Im}}$); (ii) the vibration transmissibility spectrum measured at the wrist (T_{Wrist}), which was used to represent the vibration of the palm-wrist-forearm substructures represented by M_a in the model because the wrist is at the middle location of these substructures; and (iii) the vibration transmissibility spectrum (T_{Upper}) measured on the upper arm represented by m_u in the model. The vibration transmissibility spectrum measured on the club head was not used in the model calibration, but it was used as a critical reference to validate the model for predicting the workpiece vibration. The experimental data measured on the dorsal surface of the hand and forearm were not used in this study because their corresponding substructures were not separately simulated in the model proposed in this study.

As the first step of the calibration, the modeling motion responses (**z:** z_w, z_c, z_f, z_a, z_u) were calculated using Eq. (1) with the following assumptions: $F_C = 0$; $F_W = 1 \cdot \exp^{j\omega t}$, in which $j = \sqrt{-1}$, ω is circular frequency, and t is time; and the initial values for the unknown parameters (χ: m_f, m_a, m_u, c_1, c_{f1}, c_{f2}, c_a, c_p, c_u, k_1, k_{f1}, k_{f2}, k_a, k_p, k_u), which were estimated from preliminary trials of the calibration. A unity excitation force was used in the model because the calculated response functions (impedance and transmissibility) do not vary with the force input to the linear model.

As the second step, the modeling vibration transfer function (T) relative to the input displacement (z_w), driving-point dynamic force (F_d), and mechanical impedance (Z_{Model}) were calculated from:

$$\begin{aligned} &T_L = z_L/z_w, \qquad \text{L: club head, wrist, upper arm} \\ &F_d = (z_c - z_w)\cdot(k_1 + j\omega\cdot c_1) \\ &Z_{\text{Model}} = j\omega\cdot F_d/\dot{z}_w = F_d/(j\omega\cdot z_w) \end{aligned} \tag{3}$$

As the third step, an error function $E(\chi)$ or the root-mean-square difference between the measured reference functions and their corresponding modeling functions was calculated from:

$$E(\chi) = \sum_{p=1}^{2} \alpha \sqrt{\frac{1}{22}\sum_{i=1}^{22}\left[Z_{\text{Model}-p}(\omega_i) - Z_{\text{Exp}-p}(\omega_i)\right]^2} + \sum_{L=1}^{2} \beta \sqrt{\frac{1}{22}\sum_{i=1}^{22}(\omega_i m_L)^2\cdot\left[T_{\text{Model}-L}(\omega_i) - T_{\text{Exp}-L}(\omega_i)\right]^2}, \tag{4}$$

where Z_{Model} and Z_{Exp} are the modeling and experimental impedance values, respectively; $p = 1$ for the real part of impedance; $p = 2$ for the imaginary part of impedance; T_{Model} and T_{Exp} are the magnitudes of the modeling and experimental transmissibility, respectively; $L = 1$ for wrist; $L = 2$ for upper arm; m_L is the mass value of the substructure (L) corresponding to its transmissibility (T_L); α is the weighting factor for the impedance, and β is the weighting factor for the vibration transmissibility.

The random excitation accelerations at the low frequencies (<8 Hz) are very low (<0.45 m/s^2). The measured response functions may not be reliable at such a low excitation acceleration. Some resonant vibration of the instrumented handle was also observed at very high frequencies (>1000 Hz) in some test treatments, which may also affect the quality of the experimental data at such frequencies. To avoid these uncertainties, the error integration expressed in Eq. (4) was from 8 Hz ($i = 1$) to 1000 Hz ($i = 22$) in the one-third octave bands.

Each term in Eq. (4) has the same units (N·s/m^2), and they are directly comparable. The weighting factor (α) assigned to the impedance can be the same as that (β) assigned to the transmissibility functions if they are considered equal references in the calibration. Because the measured impedance is generally more reliable than the measured transmissibility, it is recommended to assign more weighting to the impedance than 2 to the transmissibility [20]. For this reason, the normal weighting assigned to the impedance was 0.70 and that assigned to the transmissibility was 0.30 in Eq. (4). The α/β ratio was changed in the range of 1.0–4.0 (0.8/0.2) to explore their effect on the calibration results.

As the fourth step, the unknown parameters (χ) of the model were changed in sequence, and the above-described modeling calculations were repeated until the resulting error value calculated using Eq. (4) reached its minimum value. The results are the parameter values of the model for a bare hand treatment.

The last step is to determine the parameter values of the model for the gloved hand treatment from its corresponding bare hand treatment. Based on the known mechanisms of vibration-reducing gloves [12,23], their use is unlikely to significantly affect the grinding-contact properties represented by k_1 and c_1, the upper arm mass (m_u), or its connection dynamic properties represented by k_a, c_a, k_u, and c_u. To make it easy to compare and understand the modeling results, this study assumed that these parameter values remained unchanged from their corresponding bare hand treatment in the model calibration for the gloved hand treatment. Therefore, the unknown parameters (χ) for the gloved hand treatment only include m_f, m_a, c_{f1}, c_{f2}, c_p, k_{f1}, k_{f2}, k_p. Their initial values in the calibration were those of the model for the bare hand treatment. The above-described error minimization sequence was used to determine their values with the reference functions measured in the experiment for the gloved hand treatment.

2.3. Additional experiments and modeling analyses for the model evaluation

After completing the above-described experimental study, we obtained three samples of real rubber treads used in the belt grinding process at a workplace [5], as shown in Fig. 3(c). These rubber treads have different levels of hardness and are a key factor in excitation transmissibility; they are coded as R45, R55, and R65, respectively. The sample of R45 was a brand-new

tread, and its thickness was 16.5 mm. The other two samples were cut from two used drive wheels and their thickness were 17.0 mm and 11.5 mm, respectively. As shown in Fig. 3(d), a section, including one full tooth, was cut from each tread, which had the dimensions of approximately 20 mm (width) × 50 mm (length) × the thickness of each tread. Similar to that shown in Fig. 3(b), each of these tread pads was taped on the instrumented handle for simulating the grinding wheel interfaces. With these interfaces, a series of bare workpiece tests and human subject tests were conducted, using the same method as described in Section 2.2.1 and shown in Fig. 3(a and b). For the purpose of model verification, two health adult male subjects (with mean weight of 67.5 kg and mean height of 170.0 cm) participated in the experiment, none of whom participated in the reported study because those subjects were not available for this experiment. The experimental protocol was the same as that used in the previous study [21]. The test treatments included one feed force (30 N) and two hand conditions (bare hands and gloved hands). Three trials were performed for each test treatment. The experimental data measured in the bare club head test were used to determine the interface stiffness and damping coefficient (k_1 and c_1) for each of the three tread interfaces using the model calibration method described in Section 2.2.2. Then, they were used to predict the responses of the system with the changed grinding interface by replacing the k_1 and c_1 values in the model calibrated with the reported reference functions described in Section 2.2.1. The predicted responses were compared with the experimental data measured in the subject tests performed in the current study, which provided some useful information on the validity and usefulness of the model developed in this study.

3. Results

The calibrated models for all of the above-described experimental treatments and the comparisons of their response functions with experimental data are presented in this section. The presented results also include the predicted responses of the drive-wheel-workpiece-hand-arm system subjected to the excitation (F_C) at the simulated grinding interface, which were calculated using a selected model of the system.

3.1. The models of the system and their response functions excited by the vibration from the drive wheel

This study used two approaches to calibrate the model. The first approach is termed as the mean-response-based model, which is created by determining the model parameters using the mean-response functions of the ten subjects [24]. The second approach is termed as the mean-property-based model, which is created by first determining the model with the

Table 1
Parameters of the models determined based on the averaged frequency response functions of the ten subjects for the twelve combinations of three levels of interface rubber stiffness (low-R1, middle-R2, high-R3), two feed forces (15 N and 30 N), and two hand conditions (bare and gloved hands), together with the R^2-values for assessing the goodness of the average response-based model fitting to the average real and imaginary parts of the measured impedance (Z_{Re}, Z_{Im}) and the average vibration transmissibility spectra measured on club head (T_{Head}), at wrist (T_{Wrist}), and on upper arm ($T_{UpperArm}$) with ten human subjects [21]. (Bold numbers are for bare hand treatments).

ID	Unit	Low-stiffness interface (R1)				Middle-stiffness interface (R2)				High-stiffness interface (R3)			
		30 N feed force		15 N feed force		30 N feed force		15 N feed force		30 N feed force		15 N feed force	
		Bare	Gloved	Bare	Gloved	Bare	Gloved	Bare	Gloved	Bare	Gloved	Bare	Gloved
m_w	kg	**19.5**	19.5	**19.5**	19.5	**19.5**	19.5	**19.5**	19.5	**19.5**	19.5	**19.5**	19.5
m_c	kg	**0.201**	0.201	**0.201**	0.201	**0.201**	0.201	**0.201**	0.201	**0.201**	0.201	**0.201**	0.201
m_f	kg	**0.041**	0.045	**0.048**	0.053	**0.040**	0.044	**0.044**	0.049	**0.040**	0.040	**0.043**	0.050
m_a	kg	**2.112**	2.244	**2.482**	2.539	**1.749**	2.049	**1.874**	2.009	**1.624**	1.918	**1.744**	1.904
m_u	kg	**3.000**	3.000	**3.000**	3.000	**3.000**	3.000	**3.000**	3.000	**3.000**	3.000	**3.000**	3.000
k_2	N/m	**10000000**	**10000000**	**10000000**	**10000000**	**10000000**	**10000000**	**10000000**	**10000000**	**10000000**	**10000000**	**10000000**	**10000000**
k_1	N/m	**1065126**	1065126	**637753**	637753	**1678362**	1678362	**802519**	802519	**2295182**	2295182	**986927**	986927
k_{f1}	N/m	**205873**	178482	**136711**	121740	**259764**	187728	**150505**	124746	**264314**	245084	**168949**	185864
k_{f2}	N/m	**28722**	26662	**19956**	18856	**28821**	26277	**19152**	18181	**28445**	24067	**19456**	18255
k_p	N/m	**48**	36	**51**	39	**25**	23	**33**	21	**27**	20	**25**	9
k_a	N/m	**13431**	13431	**14643**	14643	**10639**	10639	**10963**	10963	**10116**	10116	**9924**	9924
k_u	N/m	**788**	788	**992**	992	**1433**	1433	**1506**	1506	**1537**	1537	**1966**	1966
c_2	N ·s/m	**200**	200	**200**	200	**200**	200	**200**	200	**200**	200	**200**	200
c_1	N ·s/m	**172.6**	172.6	**144.1**	144.1	**254.6**	254.6	**211.4**	211.4	**279.8**	279.8	**231.0**	231.0
c_{f1}	N ·s/m	**15.0**	15.0	**15.0**	15.0	**23.5**	15.0	**15.0**	15.0	**37.0**	18.0	**15.0**	15.0
c_{f2}	N ·s/m	**75.5**	75.5	**63.8**	64.4	**78.6**	73.0	**62.4**	61.4	**70.4**	70.9	**61.6**	73.4
c_p	N ·s/m	**0.0**	0.0	**0.0**	0.0	**0.0**	0.0	**0.0**	0.0	**0.0**	0.0	**0.0**	0.0
c_a	N ·s/m	**120.6**	120.6	**109.2**	109.2	**106.5**	106.5	**104.6**	104.6	**111.6**	111.6	**102.3**	102.3
c_u	N ·s/m	**151.4**	151.4	**176.4**	176.4	**109.6**	109.6	**127.7**	127.7	**101.1**	101.1	**103.0**	103.0
R^2 *value*	Z_{Re}	**0.994**	0.982	**0.984**	0.969	**0.990**	0.946	**0.978**	0.944	**0.991**	0.981	**0.978**	0.965
	Z_{Im}	**0.990**	0.978	**0.984**	0.970	**0.978**	0.951	**0.957**	0.928	**0.985**	0.976	**0.968**	0.966
	T_{Head}	**0.920**	0.917	**0.882**	0.889	**0.722**	0.566	**0.719**	0.421	**0.620**	0.521	**0.326**	0.215
	T_{Wrist}	**0.995**	0.989	**0.996**	0.987	**0.995**	0.990	**0.995**	0.984	**0.991**	0.993	**0.995**	0.993
	$T_{UpperArm}$	**0.977**	0.986	**0.969**	0.979	**0.987**	0.993	**0.984**	0.982	**0.987**	0.990	**0.990**	0.993

response functions measured with each subject, then taking the average of the individuals' parameter values [24]. The mean-response-based model parameters for each of the twelve experimental treatments are listed in Table 1, together with the R^2-values for assessing the goodness of the model response functions fit to the measured mean response functions. The comparisons of the mean-response-based modeling results and their corresponding experimental data are shown in Figs. 4–6. The parameter values and R^2-values for the mean-property-based model are listed in Table 2. As reflected from the very similar R^2-values for each test treatment listed in Tables 1 and 2, the comparisons of the mean-property-based modeling results and their corresponding experimental data for each test treatment are very similar to those shown in Figs. 4–6. The change of the weighting ratio (α/β) in the given range (1.0–4.0) did not significantly alter the calibration results.

As shown in Figs. 4–6, both the real and imaginary parts of modeling impedance matched well with the measured data for all the cases (R^2-values ≥ 0.928). Similarly, the modeling transmissibility spectra on the upper arm and at the wrist agreed well with the measured spectra (R^2-values ≥ 0.982), except that the measured transmissibility values on the wrist at

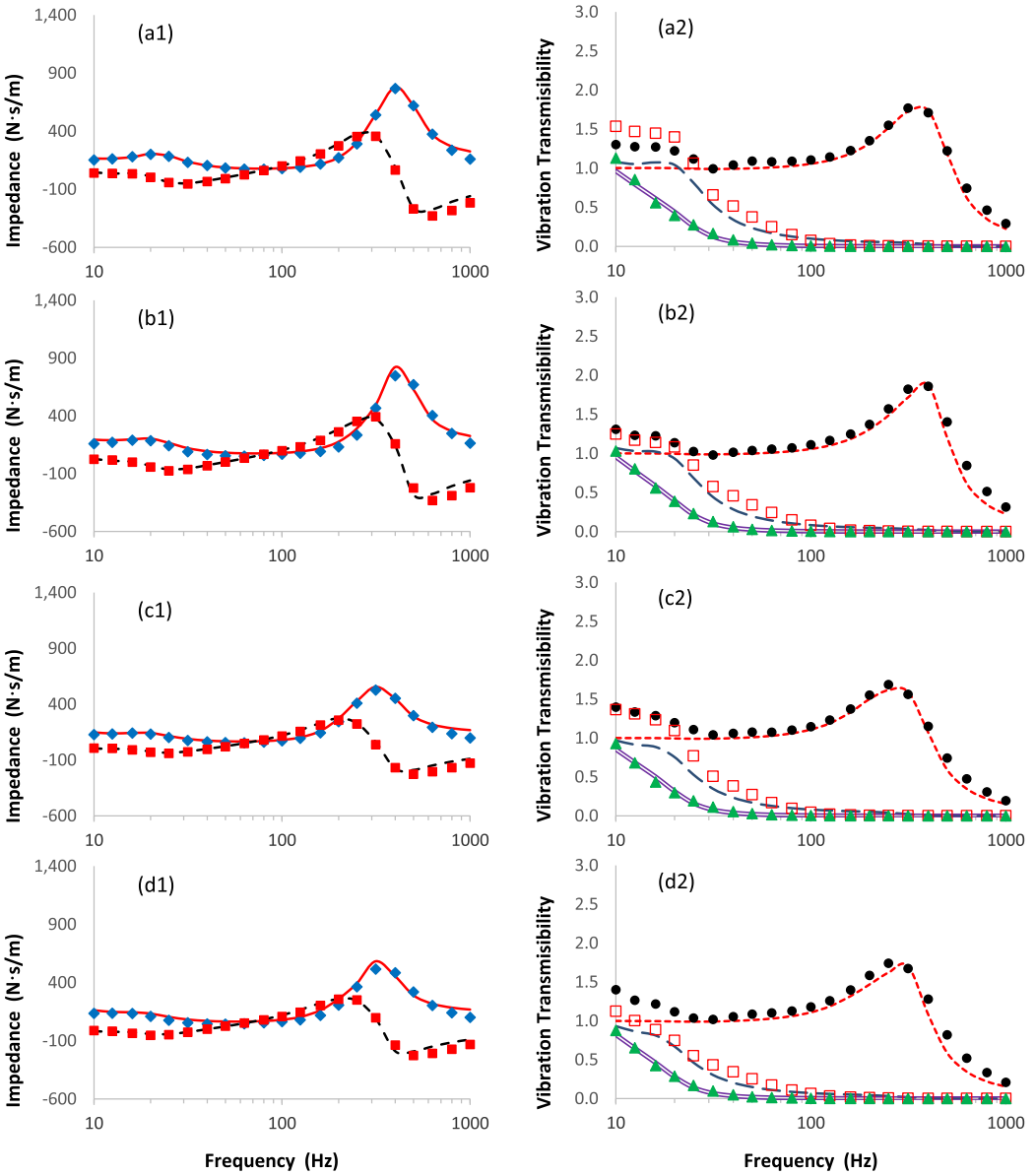

Fig. 4. Comparisons of the measured and modeling results for the low-stiffness rubber pad (R1) under four different combinations: (a) bare hands with 30 N feed force; (b) gloved hands with 30 N feed force; (c) bare hands with 15 N feed force; and (d) gloved hands with 15 N feed force. Mechanical impedances in the right column: ◆ measured real part; — simulated real part; ■ measured imaginary part; - - - simulated imaginary part. Their corresponding vibration transmissibility magnitudes in the left column: ● measured on club head; ---- prediction for club head; □ measured at wrist; ----- simulation for wrist; ▲ measured on upper arm; —— simulation for upper arm.

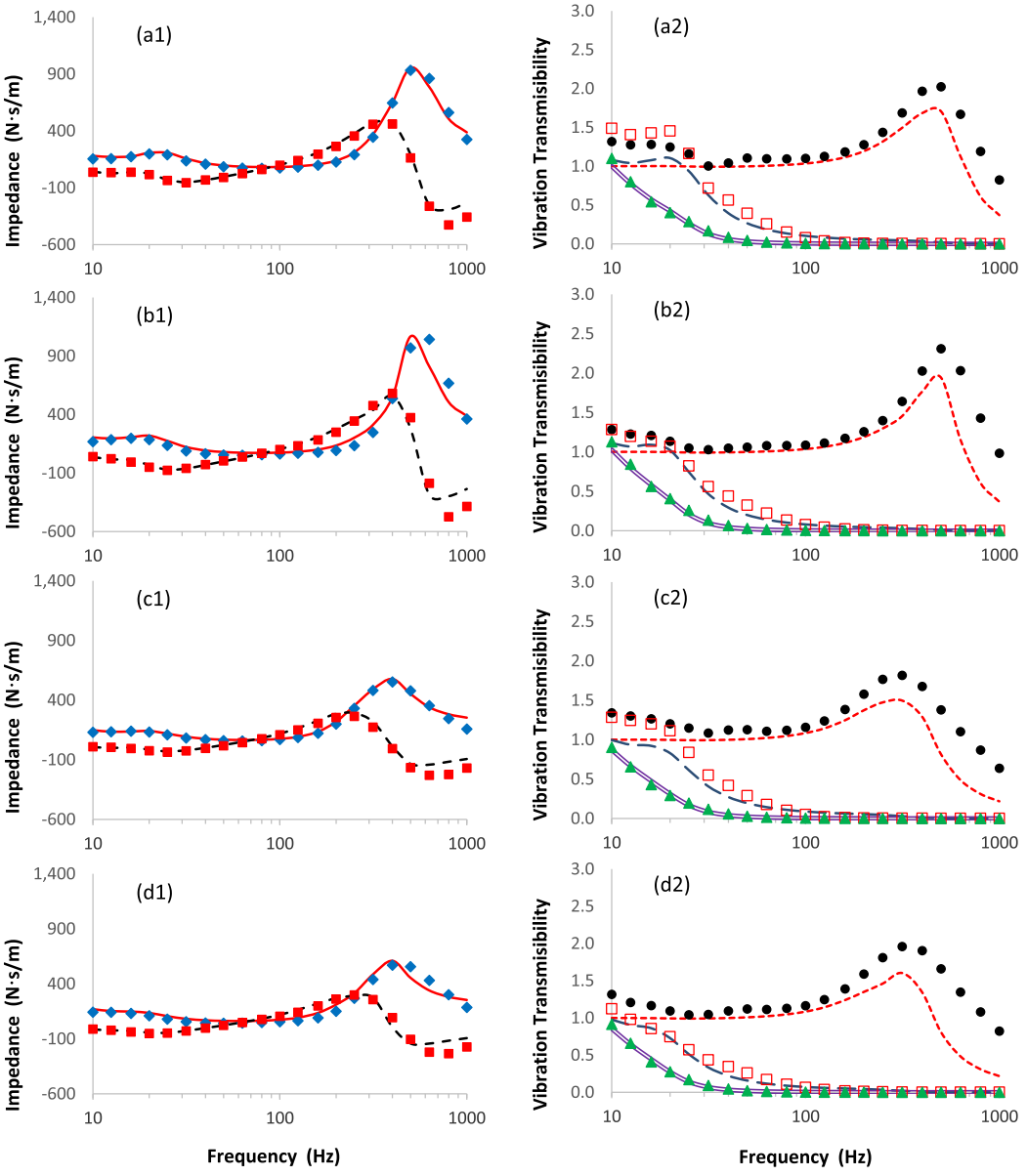

Fig. 5. Comparisons of the measured and modeling results for the middle-stiffness rubber pad (R2) under four different combinations: (a) bare hands with 30 N feed force; (b) gloved hands with 30 N feed force; (c) bare hands with 15 N feed force; and (d) gloved hands with 15 N feed force. Mechanical impedances in the right column: ◆ measured real part; —— simulated real part; ■ measured imaginary part; - - - simulated imaginary part. Their corresponding vibration transmissibility magnitudes in the left column: ● measured on club head; ---- prediction for club head; □ measured at wrist; -----6 simulation for wrist; ▲ measured on upper arm; —— simulation for upper arm.

frequencies below 25 Hz were higher than those of the modeling results. The goodness of the agreement between the predicted club head transmissibility spectrum and the measured data depended primarily on the interface rubber. In the case of low-stiffness rubber, the model provided a very reasonable prediction (R^2-values ≥ 0.879), as shown in Fig. 4. The agreement decreased for the cases of middle- and high-stiffness interfaces, as shown in Figs. 5 and 6 and reflected from the R^2-values listed in Tables 1 and 2.

The values of m_w, m_c, k_2, and c_2 were fixed in the model calibration. For the vast majority of the cases, the calibrated parameter values of the mean property-based model for each test treatment were similar to those of the mean-response-based model, with differences less than 20%. The largest differences between these two models were observed in the k_u values, which may have resulted from errors of the reference functions induced from their averaging process [24]. The observed differences, however, did not affect the general trends of the effects of the interface rubber type, feed force level, or hand glove condition on the model parameters. Because the mean-property-based model is theoretically more reliable than

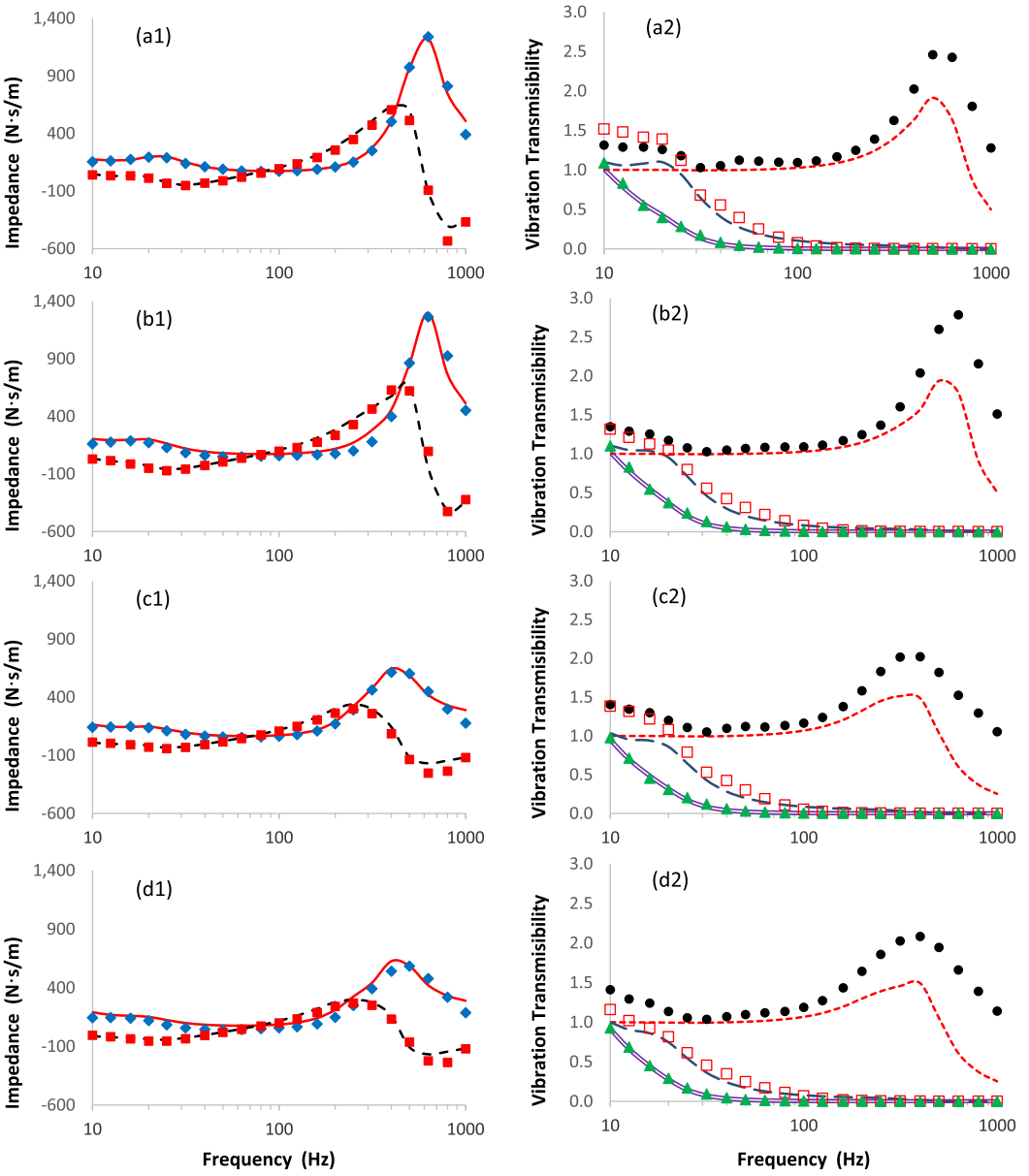

Fig. 6. Comparisons of the measured and modeling results for the high-stiffness rubber interface (R3) under four different combinations: (a) bare hands with 30 N feed force; (b) gloved hands with 30 N feed force; (c) bare hands with 15 N feed force; and (d) gloved hands with 15 N feed force. Mechanical impedances in the right column: ◆ measured real part; —— simulated real part; ■ measured imaginary part; – – – simulated imaginary part. Their corresponding vibration transmissibility magnitudes in the left column: ● measured on club head; ---- prediction for club head; □ measured at wrist; ----- simulation for wrist; ▲ measured on upper arm; —— simulation for upper arm.

the mean-response-based model [24], the specific effects are described using the results listed in Table 2 in the following presentation. This is also because the significance of each effect can be statistically analyzed using a paired t-test of the individual model parameter values of the ten subjects.

As presented in Table 2, the palm contact stiffness (k_p) and damping coefficient (c_p) are very small. This suggests that the palm is not in tight contact with the club head in the experiment; the club head was held and controlled primarily by the fingers. The m_f value was between 0.041 kg and 0.060 kg. These mass values are obviously less than the mass of the full fingers of two hands [17]; these values may represent only the effective mass of fingertips. As expected, the use of gloves generally increased the fingertip effective mass ($p \leq 0.003$) and the effective mass of the palm-wrist-forearm substructures (m_a) ($p \leq 0.003$), but glove use reduced the fingertip contact stiffness (k_{f1}) and the finger connection stiffness (k_{f2}) under the 30 N feed force ($p < 0.05$). The glove effect on k_{f2} under the 15 N feed force was suggestively significant ($p = 0.075$), but the effect on k_{f1} for this feed force was not significant ($p = 0.423$). The three interfaces under each feed force corresponded to three distinct

Table 2
Parameters of the models determined based on the averaged model properties of the ten subjects for the twelve combinations of three levels of interface rubber stiffness (low-R1, middle-R2, high-R3), two feed forces (15 N and 30 N), and two hand conditions (bare and gloved hands), together with the R^2-values for assessing the goodness of the average property-based model fitting to the average real and imaginary parts of the measured impedance (Z_{Re}, Z_{Im}) and the average vibration transmissibility spectra measured on club head (T_{Head}), at wrist (T_{Wrist}), and on upper arm ($T_{UpperArm}$) with ten human subjects [21]. (Bold numbers are for bare hand treatments).

ID	Unit	Low-stiffness interface (R1)				Middle-stiffness interface (R2)				High-stiffness interface (R3)			
		30 N feed force		15 N feed force		30 N feed force		15 N feed force		30 N feed force		15 N feed force	
		Bare	Gloved	Bare	Gloved	Bare	Gloved	Bare	Gloved	Bare	Gloved	Bare	Gloved
m_w	kg	**19.5**	19.5	**19.5**	19.5	**19.5**	19.5	**19.5**	19.5	**19.5**	19.5	**19.5**	19.5
m_c	kg	**0.201**	0.201	**0.201**	0.201	**0.201**	0.201	**0.201**	0.201	**0.201**	0.201	**0.201**	0.201
m_f	kg	**0.044**	0.050	**0.049**	0.058	**0.042**	0.045	**0.046**	0.054	**0.041**	0.050	**0.045**	0.060
m_a	kg	**2.114**	2.295	**2.283**	2.377	**1.915**	2.277	**1.936**	2.115	**1.891**	2.249	**2.092**	2.272
m_u	kg	**3.505**	3.505	**3.628**	3.628	**3.435**	3.435	**3.508**	3.508	**3.456**	3.456	**3.427**	3.427
k_2	N/m	**10000000**	**10000000**	**10000000**	**10000000**	**10000000**	**10000000**	**10000000**	**10000000**	**10000000**	**10000000**	**10000000**	**10000000**
k_1	N/m	**1070316**	1070316	**640719**	640719	**1738444**	1738444	**808452**	808452	**2301712**	2301712	**994622**	994622
k_{f1}	N/m	**204726**	182653	**134636**	127043	**259591**	210511	**156138**	129507	**266990**	273545	**176302**	188589
k_{f2}	N/m	**29020**	26216	**19795**	19020	**29132**	25789	**19768**	18491	**29584**	25179	**20164**	18917
k_p	N/m	**39**	29	**40**	28	**29**	26	**30**	20	**31**	24	**31**	20
k_a	N/m	**12162**	12162	**12838**	12838	**11394**	11394	**11611**	11611	**11645**	11645	**12430**	12430
k_u	N/m	**3072**	3072	**3152**	3152	**3169**	3169	**3353**	3353	**3319**	3319	**3245**	3245
c_2	N ·s/m	**200**	200	**200**	200	**200**	200	**200**	200	**200**	200	**200**	200
c_1	N ·s/m	**169.9**	169.9	**142.5**	142.5	**254.7**	254.7	**208.8**	208.8	**270.8**	270.8	**223.7**	223.7
c_{f1}	N ·s/m	**19.0**	20.7	**15.4**	23.6	**26.4**	18.9	**15.0**	15.0	**40.9**	36.2	**15.3**	25.9
c_{f2}	N ·s/m	**75.6**	75.9	**63.2**	65.4	**76.1**	75.0	**63.2**	63.0	**72.1**	78.4	**64.5**	72.9
c_p	N ·s/m	**0.0**	0.1	**0.0**	2.4	**0.0**	0.0	**0.0**	0.0	**0.0**	0.4	**0.0**	3.7
c_a	N ·s/m	**103.2**	103.2	**101.6**	101.6	**104.0**	104.0	**102.7**	102.7	**104.3**	104.3	**96.2**	96.2
c_u	N ·s/m	**131.0**	131.0	**156.6**	156.6	**119.4**	119.4	**130.4**	130.4	**118.3**	118.3	**126.8**	126.8
R^2 *value*	Z_{Re}	**0.993**	0.978	**0.984**	0.961	**0.992**	0.960	**0.978**	0.942	**0.991**	0.974	**0.979**	0.950
	Z_{Im}	**0.988**	0.974	**0.981**	0.963	**0.977**	0.960	**0.955**	0.928	**0.985**	0.961	**0.968**	0.959
	T_{Head}	**0.919**	0.916	**0.879**	0.892	**0.751**	0.591	**0.722**	0.425	**0.626**	0.488	**0.336**	0.196
	T_{Wrist}	**0.991**	0.986	**0.995**	0.984	**0.994**	0.989	**0.995**	0.986	**0.987**	0.991	**0.991**	0.992
	$T_{UpperArm}$	**0.988**	0.992	**0.982**	0.988	**0.986**	0.993	**0.988**	0.987	**0.985**	0.988	**0.988**	0.992
f_c	Hz	**367**		**284**		**468**		**319**		**539**		**354**	
ξ_c	1	**0.183**		**0.199**		**0.215**		**0.259**		**0.199**		**0.250**	
c_1/k_1	sec	**0.00016**		**0.00022**		**0.00015**		**0.00026**		**0.00012**		**0.00022**	

Notes: Undamped natural frequency $f_c = \frac{1}{2\pi}\sqrt{k_1/m_c}$; damping ratio $\xi_c = c_1/\sqrt{m_c \bullet k_1}$.

levels of contact stiffness (k_1) and damping (c_1) ($p < 0.001$). Their stiffn3ess sequence was consistent with their labels (low-R1, middle-R2, and high-R3); there was an inverse monotonic relationship between increasing levels of interface rubber stiffness, in which greater rubber stiffness was inversely related to vibration transmission. Reducing the feed force substantially decreased the club head contact stiffness and damping (k_1, c_1), the fingertip contact stiffness and damping (k_{f1}, c_{f1}), as well as the finger connection stiffness and damping (k_{f2}, c_{f2}) ($p < 0.009$).

The undamped natural frequency of the club head estimated from ($f_c = \frac{1}{2\pi}\sqrt{k_1/m_c}$) for each test treatment is also listed in Table 2. These natural frequency values generally correspond to the major peak frequency of the club head vibration transmissibility for each case, as shown in Figs. 4–6. This indicates that the major resonance of the club head depends primarily on the mass of the club head (m_c) and its contact stiffness (k_1). The related damping ratio ($\xi_c = c_1/\sqrt{m_c \bullet k_1}$) is also listed in Table 2. The damping ratio value depended on the interface. Reducing the feed force increased the damping ratio.

3.2. The model and response of the bare club head on the interface

The model of the club head in the test setup shown in Fig. 3(b) was established by removing the elements related to the hand-arm system from the model shown in Fig. 2. It is a 1-DOF model subjected to the excitation from its foundation. Only two parameters (k_1, c_1) are involved in the calibra3tion of such a model. They were calibrated using the measured mechanical impedance and evaluated using the transmissibility measured on the club head.

The essential information and parameters of the bare club head models for the six test treatments or interfaces (R1, R2, R3, R45, R55, and R65) are listed in Table 3, together with the estimated natural frequency of the club head, the related damping ratio, and c_1/k_1 ratio. The comparisons of the modeling and measured response functions for the three initial rubber interfaces are shown in Fig. 7, and those for the three additional rubber pads are presented in Fig. 8. Similar to those observed in Figs. 4–6, the modeling impedance functions reasonably matched with the measured data for all six cases (R^2–value ≥ 0.925). The predicted vibration transmissibility functions of the club head also reasonably agreed with the measured data for four rubber treatments (R1, R45, R55, and R65) (R^2–value ≥ 0.919), as shown in Figs. 7(a2) and 8(a2, b2, c2). The identified stiffness for these treatments was equal to or less than 1,088,776 N/m. Very interestingly, the stiffness for R1 (1,088,776 N/m) determined

Table 3
Model parameters for the bare club head test with the six interface rubber pads (R1, R2, R3, R45, R55, R65) under 30 N contact force.

ID	Unit	Lab rubber interfaces			Real tread rubber interfaces		
		R1	R2	R3	R45	R55	R65
Thickness	mm	3.0	1.6	0.85	16.5	17.0	11.5
m_c	kg	0.201	0.201	0.201	0.201	0.201	0.201
k_1	N/m	1088776	1260981	1698457	84829	160846	190819
c_1	N ·s/m	221.5	331.4	375.8	29.4	50.1	62.0
R^2 *value*	Z_{Re}	0.949	0.191	0.219	0.968	0.969	0.947
	Z_{Im}	0.966	0.954	0.925	0.947	0.940	0.987
	T_{Head}	0.949	0.191	0.219	0.948	0.947	0.919
f_c	Hz	370	399	463	103	142	155
ξ_c	1	0.237	0.329	0.322	0.112	0.139	0.158
c_1/k_1	sec	0.00020	0.00026	0.00022	0.00035	0.00031	0.00032

Notes: Undamped natural frequency $f_c = \frac{1}{2\pi}\sqrt{k_1/m_c}$; damping ratio $\xi_c = c_1/\sqrt{m_c \bullet k_1}$.

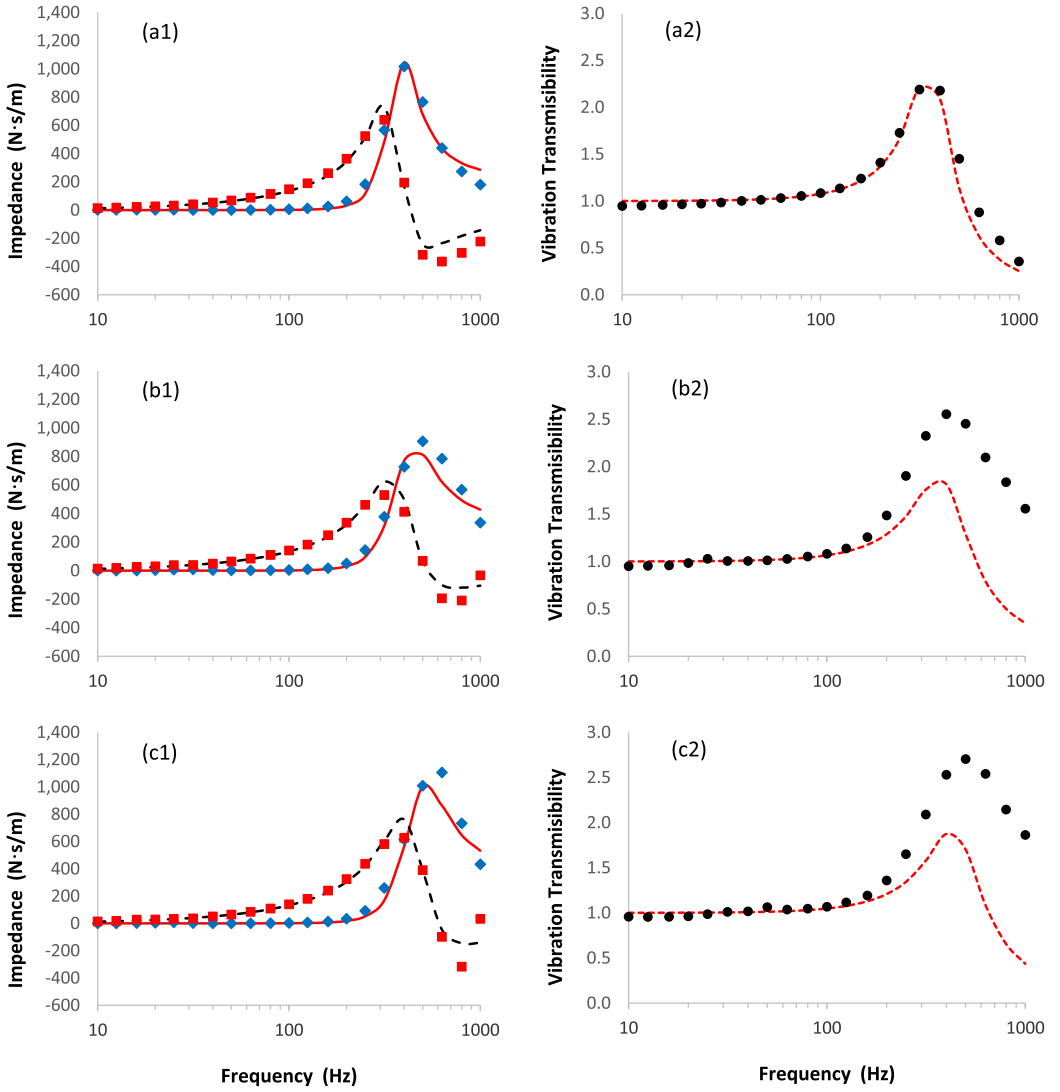

Fig. 7. Comparisons of the measured and modeling results for the bare club head test with the lab three rubber interfaces: (a) low-stiffness pad (R1); (b) middle-stiffness pad (R2); (c) high-stiffness pad (R3). Mechanical impedances in the right column: ◆ measured real part; —— simulated real part; ■ measured imaginary part; – – – simulated imaginary part. Their corresponding vibration transmissibility magnitudes in the left column: ● measured on club head; ---- prediction for club head.

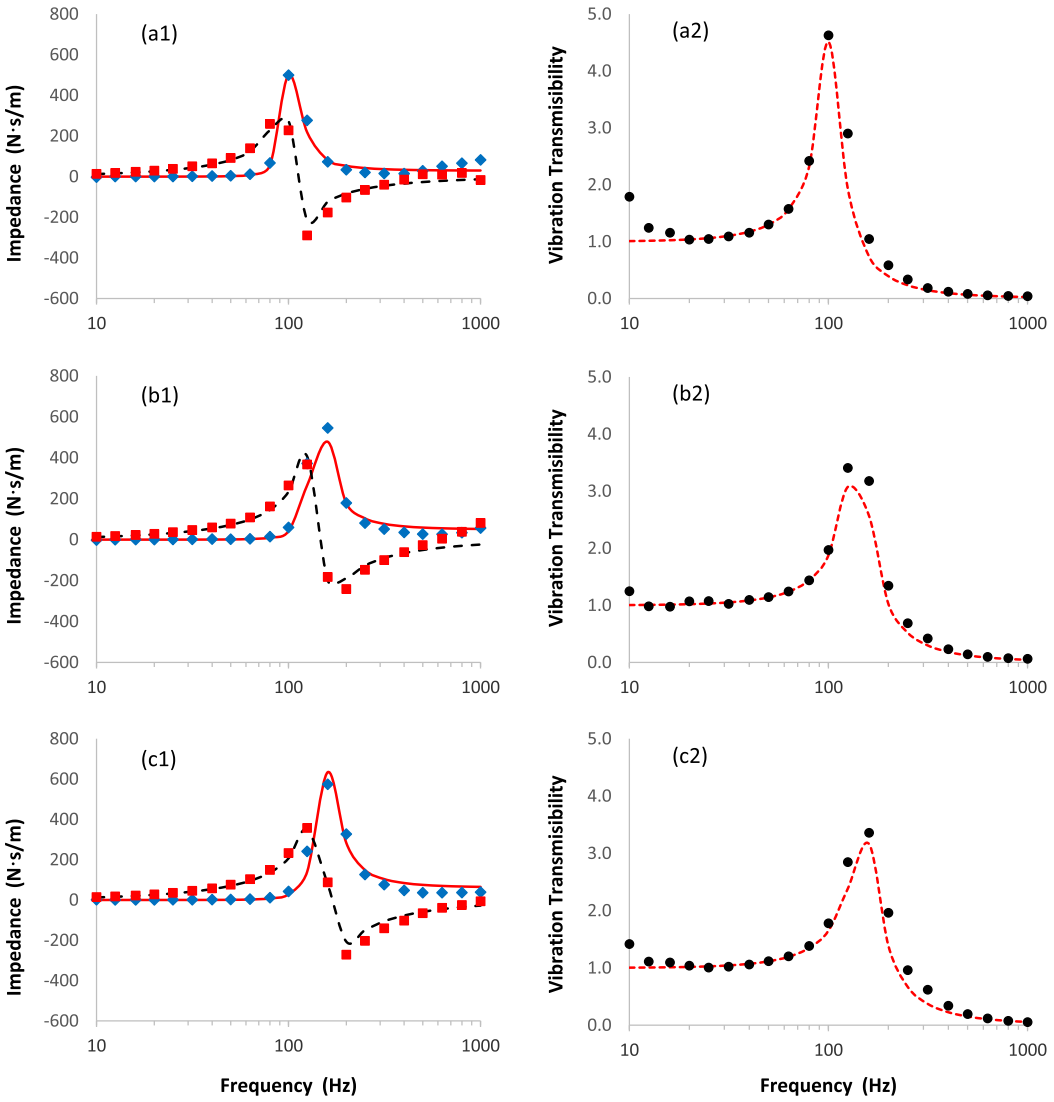

Fig. 8. Comparisons of the measured and modeling results for the bare club head test with the additional three rubber pads cut from: (a) a new rubber tire pad (R45); (b) a worn out rubber tire pad (R55); (c) another worn out rubber tire pad (R65). Mechanical impedances in the right column: ◆ measured real part; —— simulated real part; ■ measured imaginary part; – – – simulated imaginary part. Their corresponding vibration transmissibility magnitudes in the left column: ● measured on club head; ---- prediction for club head.

using the bare-workpiece-test data was very similar (difference < 1.7%) to that (1,070,316 N/m, Ta2ble 2) determined using the subject-test data. The estimated natural frequency of the bare workpiece on R1 interface (370 Hz) was also very close to that (367 Hz) of the workpiece in its coupled response of the entire interface-workpiece-hand-arm system. This indicates that the club head vibrates similarly with and without being held by the hands in such a case.

Also similar to those shown in Figs. 5 and 6, the predicted transmissibility functions of the club head had poor agreements with the measured data for the R2 and R3 treatments (R^2–value $\leq$ 0.219), as shown in Fig. 7(b2) and (c2). It was observed that the club head could not be kept at its original position by the fastening rubber bands during the test for in the R2 and R3 test treatments. This suggests that there was some separation of club head from the contact surface during the test with these rubber interfaces. Their stiffness values (1,260,981 N/m for R2 and 1,698,457 N/m for R3) were much less than those (1,738,440 N/m for R2 and 2,301,712 N/m for R3) from the subject test. The comparisons of the measured transmissibility spectra shown in Figs. 4–6 with those shown in Fig. 7 reveal that the measured resonance peak of the bare, fixed club head was generally larger than that in the human subject test.

Fig. 9 shows the measured mean driving-point mechanical impedances of the workpiece-hand-arm system on the workplace grinding wheel tread interfaces (R45, R55, and R65) (in left column of the figure) and their corresponding mean vibration transmissibility spectra on the club head and at the wrists on both hands (in the right column of the figure), together with the predicted response functions. The above-presented results suggest that the system model for R1 interface is more

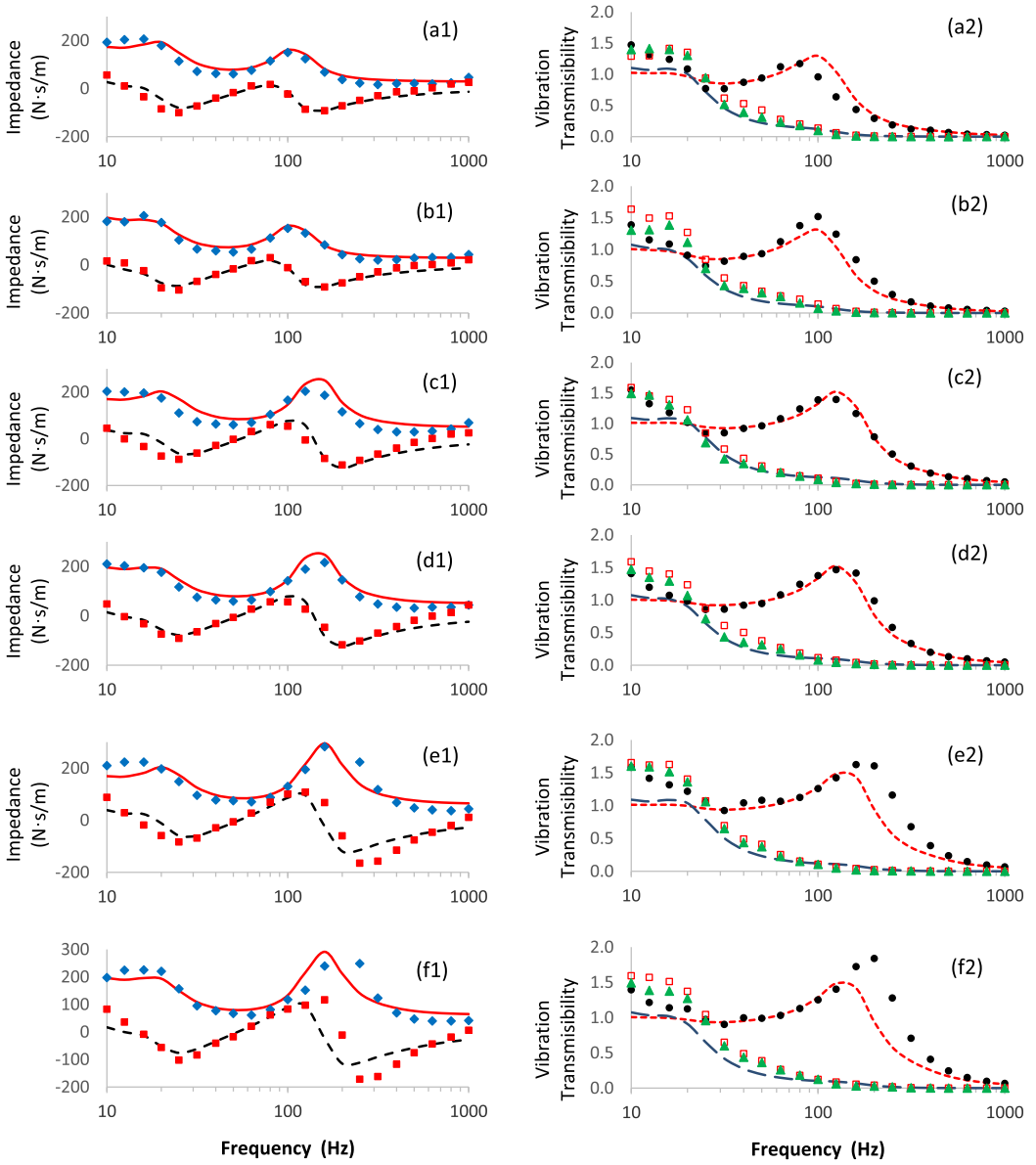

Fig. 9. Comparisons of the measured and predicted results for the three real wheel tread interfaces subjected to 30 N feed force: (a) bare hands on R45 interface; (b) gloved hands on R45 interface; (c) bare hands on R55 interface; (d) gloved hands on R55 interface; (e) bare hands on R65 interface; and (f) gloved hands on R65 interface. Mechanical impedances in the right column: ◆ measured real part; —— predicted real part; ■ measured imaginary part; – – – predicted imaginary part. Their corresponding vibration transmissibility magnitudes in the left column: ● measured on club head; - - - - prediction for club head; ----- predicted for wrist; □ measured at the left wrist; ▲ measured at the right wrist.

reliable than the models for the R2 and R3 interfaces. Therefore, the parameters of the bare hand model and gloved hand model for R1 interface under a 30 N push force listed in Table 2, except their k_1 and c_1 values, were used as a basis for the modeling predictions. The k_1 and c_1 values for each of the three workplace treads listed in Table 3 were used for the predictions of the responses on each interface. The agreements between the predicted and measured spectra were not as good as those observed in Fig. 4, but they were generally reasonable. The agreements between the predicted and measured transmissibility spectra were generally better than those for R2 and R3 shown in Figs. 5 and 6.

3.3. The predicted responses of the system subjected to the excitation acting at the grinding interface

For the above-mentioned same reason, the parameters of the four models for the R1 interface listed in Table 2 were used to predict the vibration acceleration responses of the five mass elements to a unity force excitation (1 N) at the grinding interface (F_C). The resulting acceleration spectra are presented in Fig. 10.

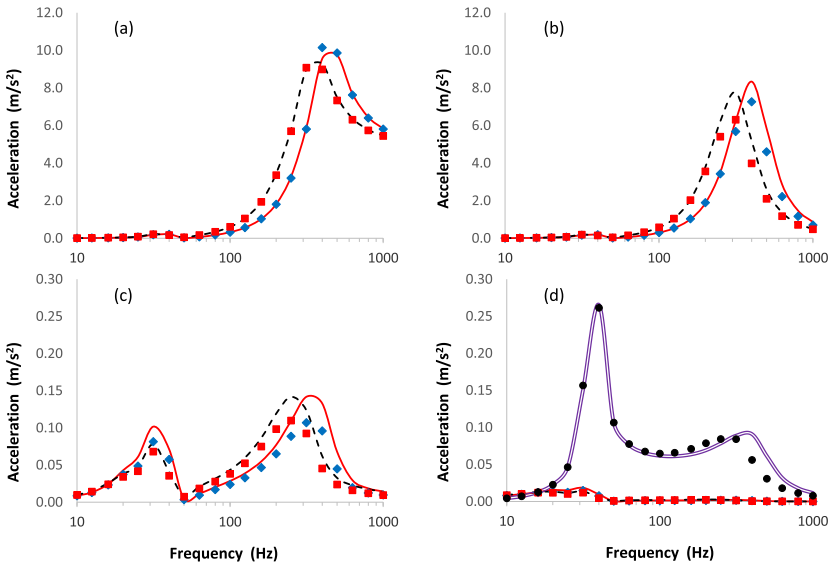

Fig. 10. The vibration acceleration responses of the system subjected to unit force excitation (1 N) on the club head in the model with the low-stiffness interface rubber under the four test treatments: —— bare hands with 30 N feed force; ◆ gloved hands with 30 N feed force; – – - bare hands with 15 N feed force; ■ gloved hands with 15 N feed force. (a) the acceleration on the handheld workpiece (m_h); (b) the acceleration on the fingertips (m_f); (c) the acceleration on the palm-wrist-forearm substructures (m_a); and (d) the acceleration on the upper arm (m_u) and that on the grinding drive wheel (m_w) (—— bare hand with 30 N feed force; and ● bare hands with 15 N feed force).

The predicted highest resonant peak is exhibited by the handheld workpiece (golf club head), as shown in Fig. 10(a). The peak frequency of the club head for each test treatment was the same as that observed in the vibration transmissibility spectra shown in Fig. 4, which can be approximately estimated from the club head mass (m_c) and its contact stiffness (k_1). As expected, the response for the treatment with a 15 N feed force had a lower peak frequency than that with a 30 N feed force because of its lower contact stiffness (k_1). The use of gloves increased the peak acceleration of the club head.

The predicted characteristics of the acceleration responses on the fingertips shown in Fig. 10(b) are similar to those on the club head shown in Fig. 10(a). This may be because the fingertips tightly held the club head, as reflected from their high contact stiffness (k_{f1}). However, the peaks were lower than those of the club head, which suggests that the fingertip contact soft tissues partially attenuated the vibration transmitted from the club head to the fingertips. As also shown in Fig. 10(b), glove use further reduced the peaks.

As shown in Fig. 10(c), there are two major resonant peaks for the mass element representing the palm-wrist-forearm substructures. The first peak is related to the fundamental resonance of these substructures. This resonance slightly affected the responses of the club head and fingertips; a minor resonance can be observed in their response spectra in the same frequency range, as shown in Fig. 10(a and b). The second peak response of these substructures is related to the club head resonance. Because of the effective cushion provided by the fingers in the high frequency range, this resonance is much less than that on the club head or fingertips. The use of gloves further reduced both peaks.

The predicted responses on the upper arm (m_u) are much less than those on any other part of the system examined in this study, as shown in Fig. 10(d). The relatively large responses shown in this figure are for the grinding drive wheel. The major peak depends primarily on the mass of the drive wheel (m_w) and the ground connection stiffness (k_2), as this resonance frequency can be approximately estimated from the values of these two parameters listed in Table 2. The parametric study on k_2 also confirmed this observation. This resonance also has some effects on the responses of the club head and the fingertips, as shown in Fig. 10(a and b). The second resonance of the drive wheel as shown in Fig. 10(d) is correlated with the club head resonance.

4. Discussion

This study developed a model of the grinding machine-workpiece-hand-arm system. The variations of the experimental treatments or conditions are reflected in the changes of the model parameters. This modeling study not only provided a useful tool for further study of the vibration control methods but also enhanced the understanding of the vibration responses of the system. The findings of this study can also be used to improve human vibration models and to apply them appropriately.

4.1. Validation and limitations of the developed model

It is emphasized that none of the vibration transmissibility spectra measured on the club head were used in the model calibrations. The agreement between the predicted transmissibility and the measured responses of the club head can thus be

used as an important criterion for the validation of the calibrated model. The results presented in Figs. 4, 7(a), 8 and 9(a-d) demonstrate that the vibration of the club head can be reasonably predicted if the grinding contact stiffness is similar to or less than that of the R1 interface listed in Tables 2 and 3. The observed effects of the interface material, feed force, and glove on the identified model parameters and the system responses are also reasonable. It is also emphasized that none of the impedance and vibration transmissibility spectra measured in the additional subject test were used in the model calibrations. The models also reasonably predicted these responses in many cases, as shown in Fig. 9(a–d). However, some large differences were observed in the comparisons of the measured and predicted transmissibility spectra of the club head, as shown in Figs. 5–7, and 9(e-f). This suggests that the models have some limitations, and their predictions may not be accurate for some cases. Nevertheless, all the presented results suggest that these models can reliably predict the basic trends of the system responses and the general effects of the influencing factors.

While the differences shown in Fig. 9 may partially result from the subject differences and the difference between the workpiece contact locations in the bare workpiece test and subject test, the differences shown in Figs. 5–7 are likely to have resulted primarily from the assumption of linearity of the system used in the simulation. This is because the dynamic forces acting at the grinding interface and the hand-club head interface actually have nonlinear relationships with the contact deformations. To help understand this error mechanism, Fig. 11 shows a nonlinear relationship between the club head contact force and the interface deformation (Δz: the relative displacement between the club head and the instrumented handle), which was constructed based on the contact stiffness (k_1) values listed in Table 2 for R1 with 15 N and 30 N feed forces. The assumed possible dynamic force range and its corresponding deformation range are also shown in the figure, together with the linear slope (k_1) at 30 N and its corresponding linear deformation range. As described in Section 2.2.1, the dynamic force is measured using an instrumented handle. For the controlled input acceleration also measured on the instrumented handle, the apparent mass or mechanical impedance used in the model calibration is proportional to the measured dynamic force. Hence, the dynamic force is actually simulated in the model calibration, and it corresponds to the linear modeling deformation shown in Fig. 11. For the nonlinear characteristics shown in the Figure, the linear deformation is always less than the actual deformation. Because the actual deformation is proportional to the measured vibration transmissibility of the club head, the measured transmissibility should also be larger than that predicted using the linear model. This explains the phenomena observed in Figs. 5–7.

The error mechanism demonstrated in Fig. 11 indicates that the prediction error increases with the increase in the degree of nonlinearity. The separation of the club head from the high-stiffness interface (R3) observed in the experiment must increase the degree of nonlinearity. This explains why the largest prediction error was observed in such a case, as shown in Figs. 6 and 7(c2). This nonlinearity error mechanism also indicates that the prediction errors increase with the increase in the vibration magnitude. Therefore, the model application should have the following two conditions: I) the stiffness of the drive wheel rubber tread should be similar to or less than that of the low-stiffness rubber (R1) used this study; and (II) the vibration magnitude of the club head is similar to or less than that observed in the measurement of the reference functions for the model calibration [21].

As indicated in Table 3, the identified stiffness values with the rubber pads (R45, R55, and R65) cut from actual grinding machine treads are much less than the stiffness of the R1 interface. This suggests that the actual drive wheel tread contact stiffness is likely to be in the required range for the model application. The root-mean-square (rms) value of the unweighted acceleration measured on the club head in the above-described laboratory experiments was in the range of 82–132 m/s^2. This range is at the high end of the total acceleration (47–149 m/s^2) measured on club heads at a workplace [5]. The frequency-weighted rms acceleration of the club head (6.5–8.1 m/s^2) measured in the laboratory experiments was also at the high end of the total weighted acceleration (3.8–8.7 m/s^2) measured at the workplace [5]. These observations suggest that the developed model is acceptable for predicting the club head vibration. This is partially confirmed from the comparisons of the experimental data and modeling predictions shown in Fig. 9.

Besides the prediction error of the club head transmissibility in its resonant frequency range, some significant differences between the modeling and experimental data can also be observed in the low frequency range (<25 Hz), as shown in Figs. 4–6

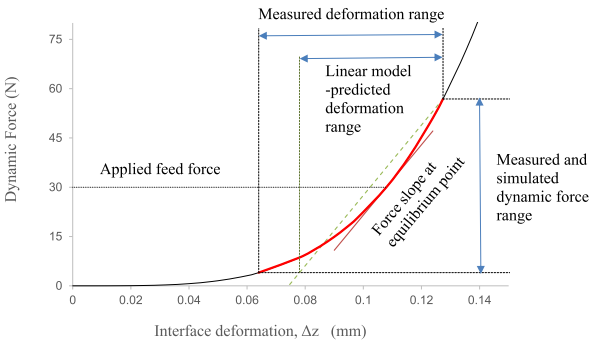

Fig. 11. The mechanism of the transmissibility prediction error of a linear contact model.

and 9. Such differences remain for all the subject test treatments. However, these differences were not observed in the bare club head test with the original three rubber interfaces, as shown in Fig. 7. Also, such differences were not evident in the measured impedance spectra, as shown in Figs. 4–6, and 9. These observations suggest that these differences are not primarily associated with the responses of club head along the z-direction, but rather from the vibrations in the other two directions. These off-axial vibrations are likely to have resulted from the cross-axial responses of the hand-arm system [25]. Some obvious cross-axial vibrations at the low frequencies were also observed in the transmissibility spectra shown in Fig. 8. This is because the rubber pads (R45, R55, and R65) cut from the workplace wheel treads do not have a uniform flat contact surface, and they are thicker and softer than R1, R2, or R3, as indicated in Table 3; club heads on such interfaces are likely to exhibit larger rocking motions than those of club heads on the R1, R2, and R3 interfaces. These observations suggest that the differences between the modeling transmissibility spectra and the measured data in the low frequency range should not affect the validity of the developed model.

4.2. Implications for the further development of system models

While the linear model developed in the current study can be used to help understand the basic characteristics of the system responses and to explore and qualitatively evaluate engineering intervention methods, it may not accurately predict the system responses when any large nonlinear behavior is present in the grinding process. Besides the above-mentioned nonlinear interface behavior, the hand-arm system may also exhibit some nonlinear behaviors. For example, the finger contact shows a large nonlinear behavior, as clearly reflected by the effect of the feed force on the finger contact stiffness (k_{f1}) identified in this study (see Tables 1 and 2). According to the error mechanism shown in Fig. 11, the linear finger contact elements (linear spring and viscous damper) used in the current study and many previous studies may largely underestimate the finger transmissibility, similar to that observed in Figs. 5 and 6. This should be one of the major reasons that the linear model-predicted finger transmissibility could be much less than the measured transmissibility, especially in the fundamental resonant frequency range of the fingers, as observed in a previous study [26]. It is anticipated that the introduction of some nonlinear elements to the system model finger can substantially improve the accuracy of the system response predictions.

Some studies claimed that the use of both vibration transmissibility and driving-point response functions could result in better models [18]. The results and observations of the current study suggest that the validity of such claims depends not only on whether the reference functions are reliably measured and the included transfer functions are representative of the motions of the substructures simulated lumped mass elements in the model [20], but also on the model structural characteristics (e.g., linear or nonlinear) and the purpose of the model. The current study attempted to include the club head transmissibility in the model calibration in the exploration of the model construction. The inclusion of such metrics reduced the predicted transmissibility errors, but it increased the simulated impedance errors in the linear model. This is because the naturally nonlinear behaviors of the system make it impossible for the linear model to fit both driving-point response functions and vibration transfer functions well. As a result, the calibrated model is actually a compromise among the inconsistent references for the linear assumption. The relative impedance/transmissibility weightings used in the model calibration determine the relative prediction errors of each response function. Therefore, the model calibration actually has no unique solution; its correct solution is application-specific. For example, the apparent mass or impedance of the hand-arm system should be solely used or accurately simulated for the analyses and designs of the grinding interfaces and powered hand tools because the impedance directly influences their vibration responses [15,16]. In such cases, it is not essential to accurately simulate the vibration transmissibility distributed on the hand-arm system. However, if the vibrations of the hand-arm system are of primary concern, it is necessary to emphasize the simulations of the actual system structure and the vibration transmissibility distributed on the system.

4.3. Implications of the model predictions

The results shown in Figs. 4–6, 9, and 10 show that the most important resonance of the system is associated with the handheld workpiece. The identified model parameters listed in Tables 1–3 indicate that such a resonance depends primarily on the mass of the club head (m_c) and the grinding contact stiffness (k_1). The results shown in Figs. 7 and 8 also suggest that this resonant frequency can be approximately identified from the bare club head test without involving in a human subject. This may provide an efficient approach for further examining this resonance on real grinding interfaces.

The resonant vibration of the club head may be effectively transmitted to the fingers, as shown in Fig. 10(b). The effect of such a resonance can be minimized in the designs or selections of the drive wheel rubber tread and the grinding sand belt. For example, a previous study found that the fundamental machine vibration is likely to be primarily associated with the unbalanced mass of the drive wheel because it is correlated with the rotation speed of the drive wheel [5]. The rotational speeds of the grinding machines examined in the reported study ranged from 20 to 40 Hz. A major component of the excitation at the grinding interface is related to the number of rubber teeth on the drive wheel tread; the excitation frequency is equal to the drive wheel rotation speed multiplied by the number of the teeth on the drive wheel tread. Hence, the fundamental interface excitation frequency should be in the range of 760 to 1,520 Hz for the large drive wheel machine with 38 wheel tread teeth and in the range of 360–720 Hz for the small drive wheel machine with 18 wheel tread teeth. Then, one of the options is to design the tread stiffness so that the major club head resonant frequency falls in a frequency range that is well above 40 Hz and well below 760 Hz for the large wheel machine and well above 40 Hz and well below 360 Hz for the small drive wheel

machine. As shown in Fig. 8, the large resonant responses of the club head on the rubber pads cut from the real treads falls approximately in the range of 60–200 Hz. This suggests that the real wheel tread stiffness is likely to be in the desired range for the tested club head under a 30 N feed force. While this study only examined the resonance of one club head on limited grinding interfaces, further studies are required to examine the resonant frequencies of various workpieces under their real working conditions.

Another option is to substantially reduce the contact stiffness so that the major resonant frequency is below 20 Hz and to increase the rotation speed of the drive wheel so that the dominant vibration frequency of the drive wheel is above 40 Hz. This may be achieved by conducting the grinding on the grinding belt away from the drive wheel tread or on a very soft grinding interface. Further studies are required to test this hypothesis and intervention method.

The drive wheel resonance shown in Fig. 10(d) varies primarily with its connection stiffness (k_2) and the mass of the wheel-shaft assembly (m_w). If this resonance falls within the fundamental vibration frequency range of the grinding machine (20–40 Hz), the machine-vibration induced from the unbalanced wheel mass will be greatly amplified. This will significantly increase not only the frequency-weighted vibration of the club head but also the vibration transmitted to the palm-wrist-arm substructures because their fundamental resonance is also in this frequency range, as shown in Fig. 10(c).

The comparisons of the resonant peaks measured in the bare club head tests shown in Fig. 8 with those measured in the subject tests shown in Fig. 9 for the same 30 N feed force reveal that the impedance of the hand-arm system can substantially reduce the resonant magnitude of the workpiece. As shown in Fig. 10, glove use marginally increased the club head vibration. This is because the hand constraint on the club head is reduced due to the reduced hand coupling stiffness, as reflected from the effects of the gloves on the values of k_{f1} and k_{f2} listed in Table 2. The gloves, however, reduced the vibration transmitted to the fingers and the palm-wrist-forearm substructures, as shown in Figs. 4–6 and 10. This suggests that the use of vibration-reducing gloves in the grinding of a handheld workpiece may have some benefits. These observations also suggest that the resonance of the club head vibration can be reduced by increasing constraints on it. Further studies are required to find how to add sufficient constraints to the handheld workpiece to reduce its vibration without affecting the grinding process quality and efficiency.

5. Conclusions

This study proposed and used an inverse dynamic approach to develop a vibration model of grinding machine-workpiece-hand-arm system using the frequency response functions of the system obtained from a previous study. Additional experiments and analyses were also performed to evaluate the developed models. The modeling results reveal that the predominant resonance of the system is associated primarily with the mass of the workpiece and its grinding contact stiffness, which can be approximately determined using the response functions measured in a bare workpiece test. While the contact stiffness can be affected by many factors, this study examined the effects of the grinding feed force and several grinding contact interfaces on the resonance. Increasing the feed force increases the contact stiffness non-linearly. The hand-arm system basically serves as an impedance or constraint on the club head to reduce the resonance of the club head. Vibration-reducing gloves marginally reduce the hand coupling or the constraint; as a result, glove use marginally increases the workpiece resonance while reducing some vibration transmitted to the hand-arm system. This study also found that by assuming linearity in important contact interface characteristics, the models developed in this study can significantly underestimate the transmitted vibration. This non-linearity error mechanism is clarified in this study, which suggests that the use of nonlinear contact models can significantly improve human vibration modeling predictions. This error mechanism also indicates that the application of the developed model should meet the following two conditions: (I) the stiffness of the drive wheel rubber tread should be below a certain value; and (II) the vibration magnitude of the club head should be limited to a certain range. The reported club head vibration data and the dynamic properties of the real wheel treads identified in this study suggest that it is not difficult to meet these conditions on a belt grinding machine. This was also confirmed from the results obtained from the additional experiments and analyses performed in this study. These observations suggest that the developed model is acceptable at least for the prediction of the basic trends of the system responses and the effects of major influencing factors on the handheld workpiece vibration. Hence, the model can be used to explore and evaluate the engineering methods for controlling vibration exposures in the grinding process of handheld workpieces on a belt grinding machine.

Disclaimers

The findings and conclusions in this paper are those of the author and do not necessarily represent the official position of the National Institute for Occupational Safety and Health, Centers for Disease Control and Prevention.

References

[1] K. Ikeda, H. Ishizuka, A. Sawada, K. Urushiyama, Vibration acceleration magnitudes of hand-held tools and workpieces, Ind. Health 36 (1998) 197–208.
[2] U. Kaulbars, Hand-arm vibration – risk assessment in dental laboratories, in: The Proceedings of the 22nd Japan Conference on Human Response to Vibration, Okinawa, Japan, 2014, pp. 5–14.

[3] Q.S. Chen, B. Xiao, A.C. Yang, H.S. Lin, H. Yan, L. Lang, M.S. Yan, G.P. Chen, F.S. Zeng, X.Q. Cao, The characteristics of vibration-induced white finger in workers polishing handheld pieces in the southern subtropics of China, in: The Proceedings of the 13th International Conference on Hand-arm Vibration, Beijing, China, 2015, pp. 19–20.
[4] ISO 5349–1, Mechanical Vibration - Measurement and Evaluation of Human Exposure to Hand-transmitted Vibration - Part 1: General Requirements, International Organization for Standardization, Geneva, Switzerland, 2001.
[5] Q. Chen, H. Lin, B. Xiao, D.E. Welcome, J. Lee, G. Chen, S. Tang, D. Zhang, G. Xu, M. Yan, H. Yan, X.S. Xu, H. Qu, R.G. Dong, Vibration characteristics of golf club heads in their handheld grinding process and potential approaches for reducing the vibration exposure, Int. J. Ind. Ergon. 62 (2017) 27–41.
[6] Y. Tominaga, New frequency weighting of hand-arm vibration, Ind. Health 43 (2005) 509–515.
[7] T. Nilsson, L. Burström, M. Hagberg, Risk assessment of vibration exposure and white fingers among platers, Int. Arch. Occup. Environ. Health 61 (1989) 473–481.
[8] L. Barregard, L. Ehrenström, K. Marcus, Hand-arm vibration syndrome in Swedish car mechanics, Occup. Environ. Med. 60 (2003) 287–294.
[9] J. Starck, P. Jussi, P. Ilmari, Physical characteristics of vibration in relation to vibration-induced white finger, Am. Ind. Hyg. Assoc. J. 51 (4) (1990) 179–184.
[10] R. Dandanell, K. Engstrom, Vibration from riveting tools in the frequency range 6 Hz-10 MHz and Raynaud's phenomenon, Scand. J. Work. Environ. Health 12 (1986) 338–342.
[11] R.G. Dong, D.E. Welcome, T.W. McDowell, X.S. Xu, K. Krajnak, J.Z. Wu, A proposed theory on biodynamic frequency weighting for hand-transmitted vibration exposure, Ind. Health 50 (5) (2012) 412–424.
[12] ISO-10068, Mechanical Vibration and Shock – Mechanical Impedance of the Human Hand-arm System at the Driving Point, International Organization of Standard, Geneva, Switzerland, 2012.
[13] M. Śledziński, Proposed model of hand for designing ergonomic vibration isolation systems for hand-held impact tools, Am. J. Mech. Eng. 2 (7) (2014) 290–294.
[14] R. Jahn, M. Hesse, Applications of hand–arm models in the investigation of the interaction between man and machine, Scand. J. Work. Environ. Health 12 (1986) 343–346.
[15] B. Saggin, D. Scaccabarozzi, M. Tarabini, Optimized design of suspension systems for hand-arm transmitted vibration reduction, J. Sound Vib. 331 (11) (2012) 2671–2684.
[16] G. Moschioni, B. Saggin, M. Tarabini, Prediction of data variability in hand-arm vibration measurements, Measurement 44 (9) (2011) 1679–1690.
[17] R.G. Dong, J.H. Dong, J.Z. Wu, S. Rakheja, Modeling of biodynamic responses distributed at the fingers and the palm of the human hand-arm system, J. Biomech. 40 (2007) 2335–2340.
[18] S. Adewusi, S. Rakheja, P. Marcotte, Biomechanical models of the human hand-arm to simulate distributed biodynamic responses for different postures, Int. J. Ind. Ergon. 42 (2012) 249–260.
[19] J. Kinne, K. Latzel, T.H. Schenk, Application of two-hand impedance as basis for mechanical modeling, in: Proceedings of the 9th International Conference on Hand-arm Vibration, Nancy, France, 2001, pp. 113–118.
[20] R.G. Dong, D.E. Welcome, T.W. McDowell, J.Z. Wu, Fundamental theory, methods, and criteria for calibrating the human vibration models using frequency response functions, J. Sound Vib. 356 (2015) 95–216.
[21] X.S. Xu, D.E. Welcome, T.W. McDowell, C. Warren, H. Lin, B. Xiao, Q. Chen, R.G. Dong, The vibration responses of a handheld workpiece and the hand-arm system, in: Proceedings of the 7th American Conference on Human Vibration, 2018 (Seattle, WA, USA).
[22] X.S. Xu, R.G. Dong, D.E. Welcome, C. Warren, T.W. McDowell, J.Z. Wu, Vibrations transmitted from human hands to upper arm, shoulder, back, neck, and head, Int. J. Ind. Ergon. 62 (2017) 1–12.
[23] ISO 10819, Mechanical Vibration and Shock - Hand-arm Vibration - Measurement and Evaluation of the Vibration Transmissibility of Gloves at the Palm of the Hand, International Organization for Standardization, Geneva, Switzerland, 2013.
[24] R.G. Dong, D.E. Welcome, T.W. McDowell, J.Z. Wu, Methods for deriving representative biodynamic response of hand-arm system to vibration, J. Sound Vib. 325 (2009) 1047–1061.
[25] R.G. Dong, S. Rakheja, W.P. Smutz, A.W. Schopper, J.Z. Wu, Evaluating anti-vibration performance of a glove using total effective transmissibility, Int. J. Ind. Ergon. 30 (2002) 33–48.
[26] R.G. Dong, D.E. Welcome, T.W. McDowell, J.Z. Wu, Modeling of the biodynamic responses distributed at the fingers and palm of the hand in three orthogonal directions, J. Sound Vib. 332 (2013) 1125–1140.